



Research articles

Curie temperature modeling of magnetocaloric lanthanum manganites using Gaussian process regression

Yun Zhang*, Xiaojie Xu

North Carolina State University, Raleigh, NC 27695, USA



ARTICLE INFO

Keywords:

Curie temperature
Gaussian process regression
Lattice parameters
Magnetocaloric effects
Manganites

ABSTRACT

Efficient solid-state refrigeration techniques have drawn increasing attention due to their potential for improving energy efficiency of refrigeration, air-conditioning, and temperature-control systems without using harmful gas as in conventional gas compression techniques. Research on magnetocaloric lanthanum manganites with near-room-temperature Curie temperature, T_C , shows promising results for further developments of magnetic refrigeration devices. By incorporating chemical substitutions, oxygen content modifications, and various synthesis methods, these manganites experience lattice distortions from perovskite cubic structures to pseudocubic, orthorhombic, and rhombohedral structures. Further changes in lattice parameters can also be achieved by the introduction of strain due to lattice mismatches, where T_C can be tuned more effectively. Empirical results and previous models through thermodynamics and first-principles have shown that changes in lattice parameters correlate with those in T_C , but correlations are merely general tendencies and obviously not universal. In this work, the Gaussian process regression model is developed to find statistical correlations between T_C and lattice parameters among lanthanum manganites. Nearly 100 lattices, cubic, pseudocubic, orthorhombic, and rhombohedral, with T_C ranging from 40 K to 375 K are explored for this purpose. The modeling approach demonstrates a high degree of accuracy and stability, contributing to efficient and low-cost estimations of T_C , providing guidance on thin film structure design and helping understandings of magnetic phase transformations and magnetocaloric effects in lanthanum manganites.

1. Introduction

Energy efficiency and sustainability are priority topics in modern society. Refrigeration and air conditioning account for a significant amount of power consumption among various end uses of energy in both commercial and residential areas [1]. Most refrigeration technology relies on the conventional gas compression (CGC) technique, which has drawn increasing criticisms due to its lack of efficiency and use of air-pollutant gas. Recent developments of magnetic refrigeration (MR) technology, based on the magnetocaloric effect (MCE) in magnetic materials particularly near room temperature, have offered an exciting alternative to vapor compression refrigeration [2]. Advantages of MR technology over CGC include, but not limited to, almost ten-fold higher cooling efficiency in magnetic refrigerators, much smaller footprints, complete solid-state operation, and being environmentally friendly [3]. Furthermore, recent developments in high-temperature superconductors with enhanced critical temperature and magnetic fields that can be generated have prompted developments of high-efficiency MR devices with superconducting magnetic field sources [4–9].

To design a magnetic refrigerator with operation temperature close to room temperature, a magnetocaloric material, with Curie temperature, T_C , near room temperature and a large magnetic entropy change, ΔS_m , over a wide temperature range, is of primary interest.

Lanthanum manganites, with the general formula, $\text{La}_{1-x-y}\text{RE}_x\text{A}_y\text{Mn}_{1-z}\text{TM}_z\text{O}_3$ (where RE is a rare earth element that partially or totally substitutes lanthanum, A is an element of the IA or IIA group, and TM is a transition element that partially substitutes Mn), are of practical importance. These materials have unique properties such as small magnetic and thermal hysteresis, a large MCE around Curie temperature T_C , and a broad working temperature range. Furthermore, manganites are inexpensive to prepare, chemically stable, and highly electrically resistive [10]. The parent LaMnO_3 compound is semiconducting and orders antiferromagnetically at 150 K, but a formation of mixed valence in Mn ions via a double exchange mechanism between Mn^{4+} and Mn^{3+} can induce ferromagnetism. A wide range of T_C from ~150 K to 375 K can be obtained by, for example, substitution of a divalent ion (Ca^{2+} , Ba^{2+} , Sr^{2+} , etc.) or a monovalent ion (Na^{1+} , K^{1+} , etc.) for La^{3+} , and an excess of oxygen. Furthermore, the ground

* Corresponding author.

E-mail addresses: yzhang43@ncsu.edu (Y. Zhang), xxu6@ncsu.edu (X. Xu).

state of manganites can be tuned by partial substitution of La^{3+} by a trivalent rare earth, or in a La-free Pr or Nd manganites. These perovskite-based structures show lattice distortions as a result of modifications from the cubic structure by the deformation of the MnO_6 octahedron arising from the Jahn-Teller effect and/or changes in the connective pattern of the MnO_6 octahedra in the perovskite structure [11–13]. Additionally, recent research on manganite superlattices and epitaxial thin films indicates that by imposing both in-plane and out-of-plane lattice strains on finite manganite layers, T_C can be tunable towards the room temperature range due to changes in lattice parameters [14–18]. There is also research suggesting that artificial oxide superlattices/multilayers might provide an alternative method to broaden ΔT_C by incorporating two types of ferromagnetic layers with lattice mismatches. Therefore, it is of great importance to investigate correlations between tunability of T_C and lattice parameters, which are results of chemical composition, chemical substitution, strain, processing condition, and different combinations of these.

Qualitative analysis on the effect of dopant types and levels on T_C of lanthanum manganites has been conducted through experiments, mainly by varying synthesis methods (solid-state reaction, wet chemistry, sol-gel, etc.), morphologies (particle size, shape, etc.), crystalline states, and final forms (powder, pellet, film, etc) [19–31]. Quantitative analysis through thermodynamics models and first-principle models has been utilized to aid the understanding of magnetothermal responses of these materials and facilitate the searching of new candidates for MR devices [32–35]. However, these models require a significant amount of data inputs, such as variables for equations of state, exchange coupling energies, and magnetic moments of magnetocaloric materials, which can only be obtained by extensive measurements.

In this work, the Gaussian process regression (GPR) model is developed to elucidate the statistical relationship between Curie temperature and lattice parameters of magnetocaloric lanthanum manganites. The model generalizes well in the presence of only a few descriptive features, where intelligent algorithms are able to learn and recognize the patterns. This modeling approach demonstrates a high degree of accuracy and stability, contributing to efficient and low-cost estimations of Curie temperature and understandings of which based on lattice parameters. As one of the computational intelligence techniques, the GPR model has already been utilized in other materials systems to predict significant physical parameters in different fields of applications [36–47]. This model can serve as a guideline for searching for bulk manganites with near-room temperature by screening the lattice parameters. It can also help design multilayer/superlattices structures that can be applied in functional micro-scale magnetic refrigeration devices. In addition, the model can be used as part of machine learning to aid understandings of magnetic phase transformations in various types of doped-manganites.

The remaining of this work is organized as follows. Section 2 proposes the GPR model. Section 3 describes the data and computational methodology. Section 4 presents and discusses results, and Section 5 concludes.

2. Proposed methodology

2.1. Brief description of Gaussian process regression

GPRs are nonparametric kernel-based probabilistic models. Consider a training dataset, $\{(x_i, y_i); i = 1, 2, \dots, n\}$ where $x_i \in \mathbb{R}^d$ and $y_i \in \mathbb{R}$, from an unknown distribution. A trained GPR predicts values of the response variable y^{new} given an input matrix x^{new} .

Recall a linear regression model, $y = x^T \beta + \epsilon$, where $\epsilon \sim N(0, \sigma^2)$. A GPR aims at explaining y by introducing latent variables, $l(x_i)$ where $i = 1, 2, \dots, n$, from a Gaussian process such that the joint distribution of $l(x_i)$'s is Gaussian, and explicit basis functions, b . The covariance function of $l(x_i)$'s captures the smoothness of y and basis functions project x into a feature space of dimension p .

A GP is defined by the mean and covariance. Let $m(x) = E(l(x))$ be the mean function and $k(x, x') = \text{Cov}[l(x), l(x')]$ the covariance function, and consider now the GPR model, $y = b(x)^T \beta + l(x)$, where $l(x) \sim GP(0, k(x, x'))$ and $b(x) \in \mathbb{R}^p$. $k(x, x')$ is often parameterized by the hyperparameter, θ , and thus might be written as $k(x, x'|\theta)$. In general, different algorithms estimate β , σ^2 , and θ for model training and would allow specifications of b and k , as well as initial values for parameters.

The current study explores two kernel functions, namely Exponential and Rational Quadratic, whose specifications are listed in Eqs. (1) and (2), respectively, where σ_l is the characteristic length scale defining how far apart x 's can be for y 's to become uncorrelated, σ_f is the signal standard deviation, $r = \sqrt{(x_i - x_j)^T(x_i - x_j)}$, and α is a positive-valued scale-mixture parameter. Note that σ_l and σ_f should be positive. This could be enforced through θ such that $\theta_1 = \log \sigma_l$ and $\theta_2 = \log \sigma_f$.

$$k(x_i, x_j|\theta) = \sigma_f^2 \exp\left(-\frac{r}{\sigma_l}\right) \quad (1)$$

$$k(x_i, x_j|\theta) = \sigma_f^2 \left(1 + \frac{r^2}{2\alpha\sigma_l^2}\right)^{-\alpha} \quad (2)$$

The Constant basis function is investigated here, whose specification is listed in Eq. (3), where.

$$B = (b(x_1), b(x_2), \dots, b(x_n))^T. \quad (3)$$

$$B = I_{n \times 1}$$

To estimate β , σ^2 , and θ , the marginal log likelihood function in Eq. (4) is to be maximized, where $K(X, X|\theta)$ is the covariance function matrix given by.

$$\begin{pmatrix} k(x_1, x_1) & k(x_1, x_2) & \dots & k(x_1, x_n) \\ k(x_2, x_1) & k(x_2, x_2) & \dots & k(x_2, x_n) \\ \vdots & \vdots & \vdots & \vdots \\ k(x_n, x_1) & k(x_n, x_2) & \dots & k(x_n, x_n) \end{pmatrix}. \quad \text{The algorithm first computes}$$

$\hat{\beta}(\theta, \sigma^2)$, maximizing the log likelihood function with respect to β given θ and σ^2 . It then obtains the β -profiled likelihood, $\log\{P(y|X, \hat{\beta}(\theta, \sigma^2), \theta, \sigma^2)\}$ where $X = (x_1, x_2, \dots, x_n)^T$, which is to be maximized over θ and σ^2 to compute their estimates.

$$\begin{aligned} \log P(y|X, \beta, \theta, \sigma^2) = & -\frac{1}{2}\{(y - B\beta)^T K(X, X|\theta) \\ & + \sigma^2 I_n\}^{-1}(y - B\beta) - \frac{n}{2}\log 2\pi \\ & - \frac{1}{2}\log |K(X, X|\theta)| + \sigma^2 I_n \end{aligned} \quad (4)$$

2.2. Performance evaluation

Performance of the proposed GPR models is evaluated using the root mean square error (RMSE), mean absolute error (MAE), and correlation coefficient (CC) in Eqs. (5)–(7) respectively, where n is the number of data points, T_i^{exp} and T_i^{est} are the i -th ($i = 1, 2, \dots, n$) experimental and estimated Curie temperature, and \bar{T}^{exp} and \bar{T}^{est} are their averages.

$$RMSE = \sqrt{\frac{1}{n} \sum_{i=1}^n (T_i^{exp} - T_i^{est})^2} \quad (5)$$

$$MAE = \frac{1}{n} \sum_{i=1}^n \left| T_i^{exp} - T_i^{est} \right| \quad (6)$$

$$CC = \frac{\sum_{i=1}^n (T_i^{exp} - \bar{T}^{exp})(T_i^{est} - \bar{T}^{est})}{\sqrt{\sum_{i=1}^n (T_i^{exp} - \bar{T}^{exp})^2 \sum_{i=1}^n (T_i^{est} - \bar{T}^{est})^2}} \quad (7)$$

Table 1
Experimental data and Curie temperature predictions.

Sample	a(Å)	b(Å)	c(Å)	Experimental Curie Temperature (K)	Predicted Curie Temperature (K)	Reference
Nd _{0.67} Ba _{0.33} Mn _{0.9} Fe _{0.1} O ₃	5.4929	7.7624	5.5207	40.00	41.39	[22]
Nd _{0.67} Ba _{0.33} Mn _{0.93} Fe _{0.07} O ₃	5.4927	7.7613	5.5203	50.00	49.27	[22]
Nd _{0.67} Ba _{0.33} Mn _{0.95} Fe _{0.05} O ₃	5.4923	7.7609	5.5201	61.00	62.64	[22]
Pr _{0.7} Ca _{0.3} Mn _{0.9} Fe _{0.1} O ₃	5.4319	7.6753	5.4646	80.00	80.83	[29]
Pr _{0.7} Ca _{0.3} Mn _{0.95} Fe _{0.05} O ₃	5.4321	7.6743	5.4648	89.95	89.80	[30]
Pr _{0.8} Na _{0.2} MnO ₃	5.4460	5.4481	7.7113	92.00	92.84	[20]
La _{0.5} Sm _{0.2} Sr _{0.3} Mn _{0.8} Fe _{0.15} O ₃	5.5038	7.7388	5.4746	94.00	95.23	[19]
Pr _{0.7} Ca _{0.3} Mn _{0.95} Co _{0.05} O ₃	5.4299	7.6696	5.4572	104.97	106.52	[30]
Pr _{0.7} Ca _{0.3} Mn _{0.98} Co _{0.02} O ₃	5.4303	7.6729	5.4599	106.00	105.89	[31]
Pr _{0.7} Ca _{0.3} Mn _{0.95} Co _{0.05} O ₃	5.4314	7.6711	5.4591	107.50	107.58	[31]
Pr _{0.7} Ca _{0.3} Mn _{0.95} Ni _{0.05} O ₃	5.4295	7.6708	5.4508	109.97	110.66	[30]
Pr _{0.6} Ca _{0.1} Sr _{0.3} Mn _{0.025} Fe _{0.075} O ₃	5.4427	5.4669	7.6919	112.00	112.79	[25]
Pr _{0.7} Ca _{0.3} Mn _{0.9} Co _{0.1} O ₃	5.4306	7.6705	5.4484	116.00	115.97	[29]
Pr _{0.7} Ca _{0.3} Mn _{0.9} Co _{0.1} O ₃	5.4306	7.6705	5.4484	116.00	115.97	[31]
Pr _{0.7} Ca _{0.3} Mn _{0.9} Ni _{0.01} O ₃	5.4328	7.6892	5.4195	118.00	118.44	[29]
La _{0.7} Sr _{0.25} Na _{0.05} Mn _{0.7} Ti _{0.2} O ₃	5.5312	5.5312	13.4161	125.00	126.23	[60]
La _{0.6} Pr _{0.1} Ba _{0.3} Mn _{0.7} Ni _{0.3} O ₃	5.4813	7.6853	5.4519	131.00	131.53	[28]
Nd _{0.67} Ba _{0.33} Mn _{0.98} Fe _{0.02} O ₃	5.4917	7.7602	5.5196	131.00	129.89	[22]
Pr _{0.1} Sm _{0.45} Sr _{0.45} MnO ₃	5.4427	5.4415	7.6800	132.00	132.43	[26]
Pr _{0.8} Na _{0.05} K _{0.15} MnO ₃	5.5641	5.4661	7.7374	134.00	134.69	[20]
La _{0.5} Sm _{0.2} Sr _{0.3} Mn _{0.8} Fe _{0.1} O ₃	5.5027	7.7403	5.4740	136.00	136.20	[19]
Pr _{0.7} Ca _{0.3} Mn _{0.95} Cr _{0.05} O ₃	5.4300	7.6679	5.4572	139.70	144.46	[30]
Pr _{0.7} Ca _{0.3} Mn _{0.9} Cr _{0.1} O ₃	5.4293	7.6691	5.4552	150.00	154.41	[29]
Nd _{0.67} Ba _{0.33} MnO ₃	5.4915	7.7591	5.5519	150.00	150.05	[22]
Pr _{0.7} Ca _{0.3} Mn _{0.95} Cr _{0.05} O ₃	5.4300	7.6679	5.4572	150.00	144.46	[21]
Pr _{0.8} Sr _{0.2} MnO ₃	5.4893	5.4795	7.7413	150.00	150.71	[50]
Pr _{0.6} Lao _{0.5} Sr _{0.2} MnO ₃	5.4937	5.4634	7.7656	150.00	150.63	[50]
La _{0.7} Sr _{0.25} Na _{0.05} Mn _{0.9} Ti _{0.1} O ₃	5.5271	5.5271	13.4021	155.00	155.78	[60]
La _{0.57} Nd _{0.1} Sr _{0.33} Mn _{0.8} Sn _{0.2} O ₃	5.5598	5.5598	13.5755	158.00	158.79	[70]
Pr _{0.7} Ca _{0.3} Mn _{0.9} Cr _{0.1} O ₃	5.4293	7.6691	5.4552	160.00	154.41	[21]
La _{0.6} Pr _{0.1} Ba _{0.3} Mn _{0.9} Ni _{0.1} O ₃	5.5032	7.7200	5.4690	162.00	162.82	[28]
La _{0.8} Ca _{0.1} □ _{0.1} MnO ₃	5.5050	7.7866	5.5255	179.00	179.18	[24]
La _{0.8} Ca _{0.15} □ _{0.05} MnO ₃	5.5066	7.7937	5.5084	181.00	181.11	[24]
Pr _{0.2} Sm _{0.35} Sr _{0.45} MnO ₃	5.4533	5.4380	7.6786	182.52	182.69	[26]
La _{0.8} Ca _{0.2} MnO ₃	5.4972	7.7771	5.5149	183.00	182.87	[24]
Pr _{0.6} Ca _{0.1} Sr _{0.3} Mn _{0.95} Fe _{0.05} O ₃	5.4382	5.4632	7.6826	185.00	187.20	[25]
La _{0.57} Nd _{0.1} Sr _{0.33} Mn _{0.865} Sn _{0.15} O ₃	5.5481	5.5481	13.4912	187.00	188.47	[70]
La _{0.67} Ca _{0.33} Mn _{0.75} Cr _{0.25} O ₃	5.4419	7.6921	5.4608	189.00	189.03	[27]
(La _{0.7} Pr _{0.3}) _{0.8} Sr _{0.2} Mn _{0.9} Co _{0.1} O _{2.97}	5.5031	7.7836	5.5238	203.00	202.76	[62]
La _{0.6} Pr _{0.1} Sr _{0.3} Mn _{0.9} Fe _{0.1} O ₃	5.4983	5.4983	13.3410	205.00	206.13	[54]
(La _{0.7} Pr _{0.3}) _{0.8} Sr _{0.2} Mn _{0.9} Co _{0.1} O _{3.02}	5.4737	7.7432	5.5148	205.00	205.04	[62]
(La _{0.7} Pr _{0.3}) _{0.8} Sr _{0.2} Mn _{0.9} Co _{0.1} O _{3.01}	5.4743	7.7443	5.5148	205.00	205.08	[62]
La _{0.7} Ca _{0.3} Mn _{0.9} □ _{0.1} O ₃	5.4410	7.6970	5.4340	206.75	206.53	[65]
La _{0.7} Sr _{0.3} Mn _{0.5} Ti _{0.1} O ₃	5.5256	5.5256	13.3899	210.00	210.08	[58]
La _{0.6} Pr _{0.1} Ba _{0.3} MnO ₃	5.5121	7.7508	5.4859	215.00	214.79	[28]
La _{0.67} Ca _{0.33} Mn _{0.9} Cr _{0.1} O ₃	5.4486	7.7000	5.4673	215.00	214.86	[27]
La _{0.57} Nd _{0.1} Sr _{0.33} Mn _{0.9} Sn _{0.1} O ₃	5.5394	5.5394	13.4236	224.00	224.78	[70]
Pr _{0.3} Sm _{0.25} Sr _{0.45} MnO ₃	5.4623	5.4387	7.6779	225.42	225.40	[26]
Pr _{0.6} Ca _{0.1} Sr _{0.3} Mn _{0.75} Fe _{0.025} O ₃	5.4384	5.4624	7.6776	235.00	233.61	[25]
La _{0.8} Ca _{0.2} MnO ₃	5.4821	7.7536	5.5128	236.50	236.22	[67,68]
La _{0.7} □ _{0.1} Ca _{0.2} MnO ₃	5.4794	7.7500	5.5082	241.00	240.73	[67,68]
La _{0.7} Ca _{0.3} MnO ₃	5.4520	5.4630	7.6850	243.00	242.53	[69]
La _{0.67} Ca _{0.33} Mn _{0.98} Ni _{0.02} O ₃	5.4545	5.4545	13.3922	244.00	244.28	[61]
La _{0.5} Sm _{0.2} Sr _{0.3} Mn _{0.95} Fe _{0.05} O ₃	5.5036	7.7252	5.4678	253.00	252.12	[19]
Pr _{0.4} Sm _{0.15} Sr _{0.45} MnO ₃	5.4718	5.4399	7.6773	261.10	260.90	[26]
Pr _{0.6} Ca _{0.1} Sr _{0.3} MnO ₃	5.4375	5.4647	7.6814	270.00	268.47	[25]
Pr _{0.5} Na _{0.05} Sr _{0.45} MnO ₃	5.4772	5.4420	7.6441	270.00	269.79	[23]
La _{0.88} Sr _{0.17} MnO ₃	5.5400	5.5400	13.3800	270.00	269.95	[55]
La _{0.7} Ca _{0.25} Sr _{0.05} MnO ₃	5.4820	5.4910	7.7210	271.00	270.63	[69]
Pr _{0.5} K _{0.05} Sr _{0.45} MnO ₃	5.4825	5.4429	7.6503	275.00	274.70	[23]
La _{0.5} Sm _{0.2} Sr _{0.3} MnO ₃	5.5019	7.7321	5.4696	278.00	276.80	[19]
La _{0.62} Eu _{0.05} Sr _{0.3} Mn _{0.85} Cr _{0.15} O ₃	5.5108	5.5108	13.3704	278.00	278.35	[51]
La _{0.8} Ba _{0.1} Ca _{0.1} Mn _{0.97} Fe _{0.03} O ₃	5.5527	5.5527	13.4674	281.00	280.90	[57]
La _{0.57} Nd _{0.1} Sr _{0.33} Mn _{0.95} Sn _{0.05} O ₃	5.4951	5.4951	13.3520	282.00	282.57	[70]
La _{0.6} Bi _{0.1} Sr _{0.25} Ca _{0.05} Mn _{0.9} Cu _{0.1} O ₃	5.4962	5.4962	13.3346	290.00	290.37	[52]
La _{0.6} Nd _{0.1} (CaSr) _{0.3} Mn _{0.9} V _{0.1} O ₃	5.4122	5.4122	13.2984	298.00	297.82	[56]
La _{0.6} Bi _{0.1} Sr _{0.3} Mn _{0.9} Cu _{0.1} O ₃	5.5063	5.5063	13.3636	300.00	303.17	[52]
La _{0.7} Ba _{0.3} Mn _{0.9} Cr _{0.1} O ₃	5.5040	5.5040	13.3597	305.00	305.41	[71]
La _{0.8} Ag _{0.2} MnO ₃	5.1780	5.1780	13.2330	306.20	305.93	[48]
La _{0.65} Eu _{0.05} Sr _{0.3} Mn _{0.9} Cr _{0.1} O ₃	5.5123	5.5123	13.3770	310.00	309.74	[51]
La _{0.7} Ca _{0.2} Sr _{0.1} MnO ₃	5.4980	5.5080	7.7310	312.00	311.39	[69]
La _{0.7} Pb _{0.3} Mn _{0.9} Ru _{0.1} O ₃	5.5372	5.5372	13.4117	313.00	312.61	[49]

(continued on next page)

Table 1 (continued)

Sample	a(Å)	b(Å)	c(Å)	Experimental Curie Temperature (K)	Predicted Curie Temperature (K)	Reference
La _{0.67} Ba _{0.33} Mn _{0.98} Ti _{0.02} O ₃	3.9119	3.9119	3.9119	314.00	313.99	[64]
La _{0.7} Sr _{0.3} Mn _{0.9} Cr _{0.1} O ₃	5.4990	5.4990	13.5050	315.00	315.08	[71]
La _{0.57} Dy _{0.1} Pb _{0.33} MnO ₃	5.5430	5.5430	13.4657	317.00	316.50	[72]
La _{0.7} Pb _{0.3} Mn _{0.9} Cr _{0.1} O ₃	5.5220	5.5220	13.5350	320.00	319.87	[71]
La _{0.7} Sr _{0.3} Mn _{0.9} Cu _{0.1} O	5.4952	5.4952	13.3437	320.00	319.49	[52]
La _{0.7} Ca _{0.15} Sr _{0.15} MnO ₃	5.5140	5.5160	7.7610	325.00	324.38	[69]
La _{0.6} Pr _{0.1} Sr _{0.3} MnO ₃	5.4953	5.4953	13.3367	329.00	328.64	[54]
La _{0.7} Ba _{0.3} MnO ₃	5.5130	5.5130	13.5270	335.00	334.75	[71]
La _{0.7} Pb _{0.3} Mn _{0.8} Ru _{0.2} O ₃	5.5365	5.5365	13.4237	335.00	334.15	[49]
La _{0.7} Pb _{0.3} MnO ₃	5.5176	5.5176	13.4116	336.00	335.50	[49]
La _{0.7} Ca _{0.1} Sr _{0.2} MnO ₃	5.4960	5.4960	13.3190	342.00	341.37	[69]
La _{0.85} Li _{0.15} SrMn ₂ O _{5+d}	3.8591	3.8591	3.8591	345.00	344.91	[63]
(La _{0.9} Er _{0.1}) _{0.67} Pb _{0.33} MnO ₃	5.4600	7.7900	5.5800	349.00	348.00	[53]
La _{0.67} Ba _{0.33} MnO ₃	3.9075	3.9075	3.9075	350.00	349.60	[64]
La _{0.7} Pb _{0.3} MnO ₃	5.5240	5.5240	13.5680	353.00	352.46	[71]
La _{0.9} Li _{0.1} SrMn ₂ O _{5+d}	3.8601	3.8601	3.8601	355.00	354.87	[63]
(La _{0.56} Ce _{0.14}) Sr _{0.3} MnO ₃	5.5037	5.5037	13.3452	357.00	356.30	[59]
La _{0.95} Li _{0.05} SrMn ₂ O _{5+d}	3.8611	3.8611	3.8611	360.00	359.68	[63]
La _{0.67} Pb _{0.33} MnO ₃	5.5487	5.5487	13.4735	360.00	358.49	[72]
La _{0.7} Sr _{0.25} Na _{0.05} MnO ₃	5.5062	5.5062	13.3602	363.00	359.49	[60]
La _{0.7} Sr _{0.3} MnO ₃	5.4990	5.4990	13.5440	370.00	369.42	[71]
La _{0.67} Sr _{0.33} MnO ₃	5.4879	5.4879	13.3622	375.00	374.36	[66]
Mean	5.3966	6.2819	8.6892	226.17	226.17	–
Median	5.4920	5.5292	7.6783	224.71	225.09	–
Standard Deviation	0.3647	1.2194	3.6970	91.26	90.86	–
Minimum	3.8591	3.8591	3.8591	40.00	41.39	–
Maximum	5.5641	7.7937	13.5755	375.00	374.36	–
Correlation Coefficient with Experimental Curie Temperature	–27.85%	–63.07%	50.28%		99.99%	–

Notes: “ $a(\text{\AA})$,” “ $b(\text{\AA})$,” and “ $c(\text{\AA})$ ” are lattice parameters. “Predicted Curie Temperature (K)” shows the result from the current work, meaning predicted values based on the Gaussian process regression. “Experimental Curie Temperature (K)” and “Predicted Curie Temperature (K)” are visualized in Fig. 3.

3. Empirical study

3.1. Description of dataset

The experimental data used, shown in Table 1 (Columns 1–5), are obtained from [19,48–51,20,21,52–57,22,23,58,59,24,60,61,25,62,26,63,27,64,28,65,66,29–31,67–72]. The dataset covers a wide range of doped-lanthanum manganites in the form of bulk polycrystalline, single crystal, powders, and sintered pellets, by different synthesis routes, including solid-state reactions, wet-mix processing, and sol-gel processing. Nearly 100 lattices, cubic, pseudocubic, orthorhombic and rhombohedral, with T_c ranging from 40 K to 375 K are explored. Data visualization in Fig. 1 reveals nonlinear relationships, which are modeled through the GPR.

3.2. Computational methodology

MATLAB is utilized for computations and simulations in this work. The relationship between model performance and training data sizes is first investigated in Fig. 2, which shows the benefit of training the GPR using all observations. The stability of the GPR approach is confirmed by bootstrap analysis.

4. Result and discussion

4.1. Prediction accuracy

The final GPR model is detailed in Fig. 3, which shows good alignment between predicted and experimental data. The CC, RMSE, and MAE are 99.99%, 1.3453, and 0.7869, respectively, representing good prediction performance.

4.2. Prediction stability

Given the relatively small sample size (see Table 1) used, the prediction stability of the GPR is assessed through bootstrap analysis in Fig. 4, which shows that the modeling approach maintains high CCs, low RMSEs, and low MAEs over the bootstrap samples. This result suggests that the GPR might be generalized for Curie temperature modeling of magnetocaloric lanthanum manganites based on larger samples.

4.3. Prediction sensitivity

Table 2 and Fig. 3 show that GPR predictions are not so sensitive to choices of kernels considered. However, it is worth noting that estimated model parameters are different across these kernels.

5. Conclusion

The Gaussian process regression (GPR) model is developed to predict Curie temperature of magnetocaloric lanthanum manganites based on lattice parameters. The high correlation coefficient between the predicted and experimental Curie temperature, the low prediction root mean square error and mean absolute error, and stable model performance suggest the usefulness of the GPR for modeling and understanding the relationship between lattice parameters and Curie temperature. This modeling approach is straightforward and simple, which requires fewer parameters as compared to many other modeling methods. It can be used as part of computational intelligence approaches for new magnetocaloric materials searches and new multi-layer thin film structure design.

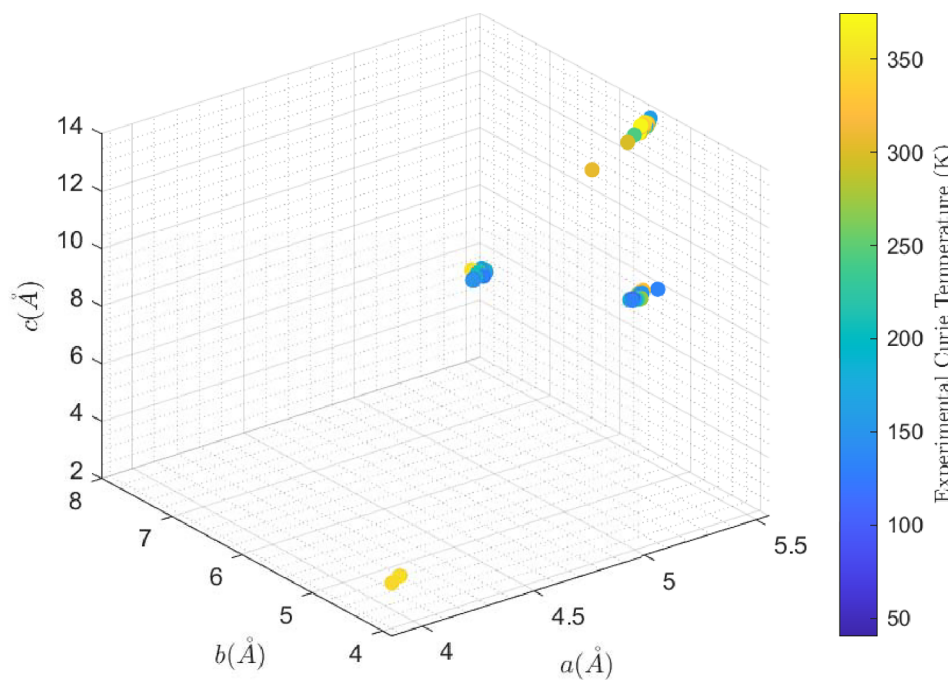


Fig. 1. Curie temperature and lattice parameters, $a(\text{\AA})$, $b(\text{\AA})$, and $c(\text{\AA})$.

Declaration of Competing Interest

The authors declare that they have no known competing financial interests or personal relationships that could have appeared to influence the work reported in this paper.

CRediT authorship contribution statement

Yun Zhang: Conceptualization, Data curation, Investigation, Methodology, Writing - original draft, Writing - review & editing.
Xiaojie Xu: Formal analysis, Visualization, Software.

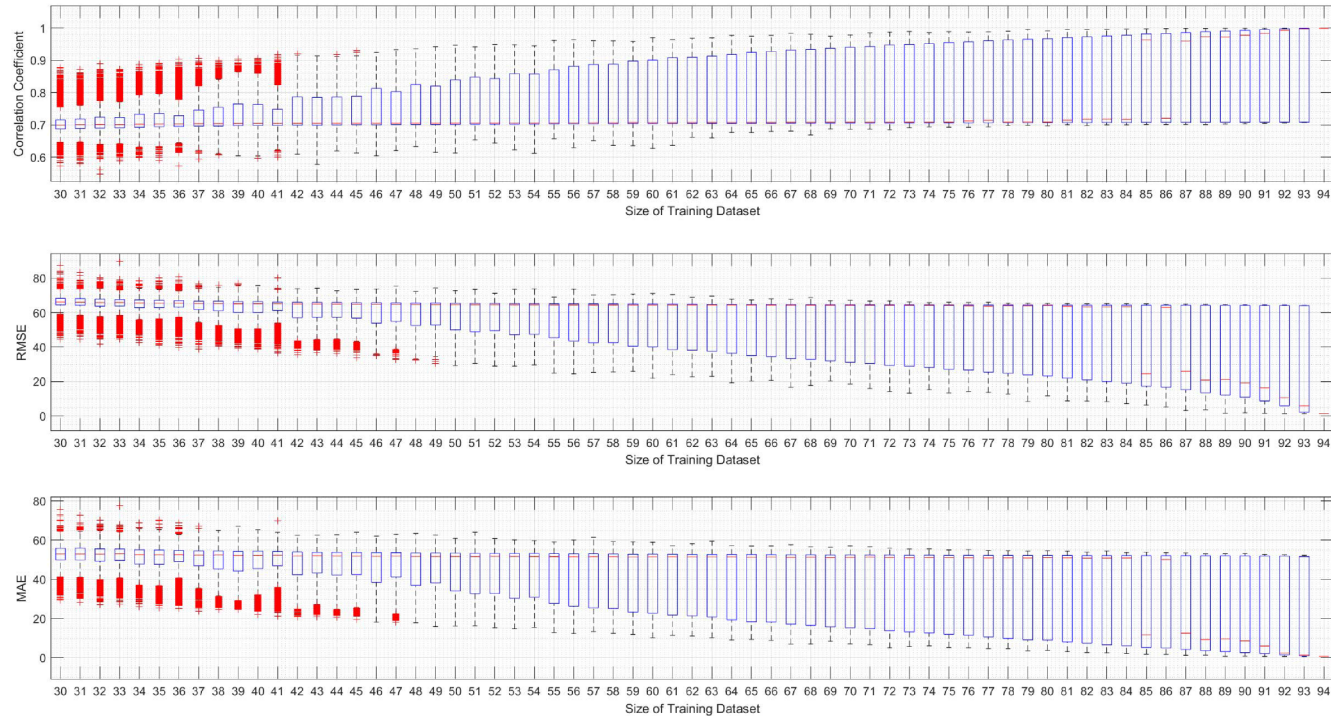


Fig. 2. Model performance and training data sizes. When the training dataset size is between 30 and 92, 2000 random sub-samples are drawn without replacements from the whole sample for model training. When the training dataset size is 93 or 94, ${}_{94}\text{C}_{93}$ or ${}_{94}\text{C}_{94}$ sub-samples are drawn without replacements from the whole sample based on exhaustive sampling for model training. Each trained model based on a certain sub-sample is used to score the whole sample and obtain the associated model performance. The GPR here uses the Rational Quadratic kernel and Constant basis function. Given a model performance measure, box plots show the median, 25th percentile, and 75th percentile. The whiskers extend to the most extreme values (i.e. ± 2.7 standard deviation coverage) not considered as outliers, and the outliers are plotted using the "+" symbol.

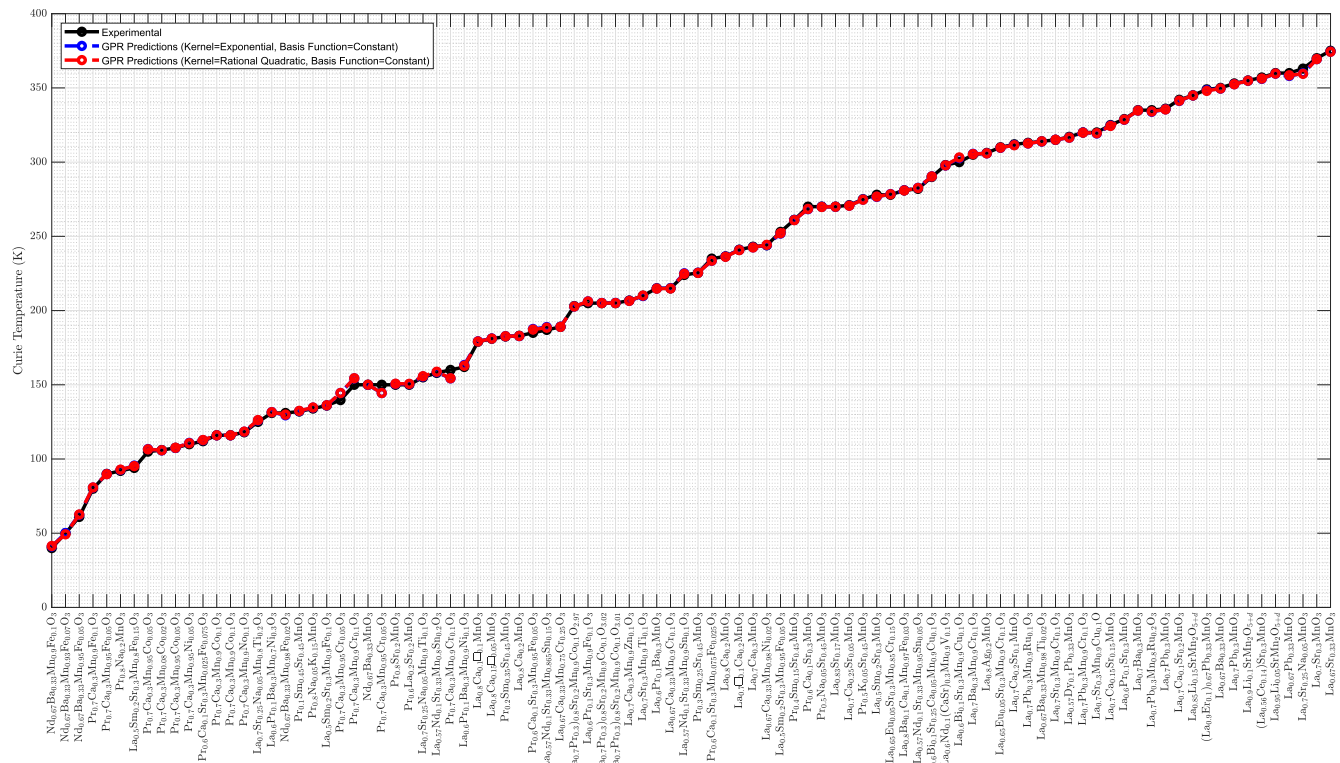


Fig. 3. Experimental vs. predicted Curie temperature. The final GPR model is built using the whole sample with the Rational Quadratic kernel, Constant basis function, and standardized lattice parameters. It has a log-likelihood of -514.4729 , $\hat{\beta}$ of 254.4081 , $\hat{\sigma}$ of 6.1111 , $\hat{\alpha}_l$ of 0.0031 , $\hat{\alpha}_f$ of 87.3150 , and $\hat{\alpha}$ of 0.1382 . Detailed numerical predictions are listed in [Table 1](#) (Column 6). Model performance of the GPR model based on the Exponential kernel and Constant basis function is detailed in [Table 2](#).

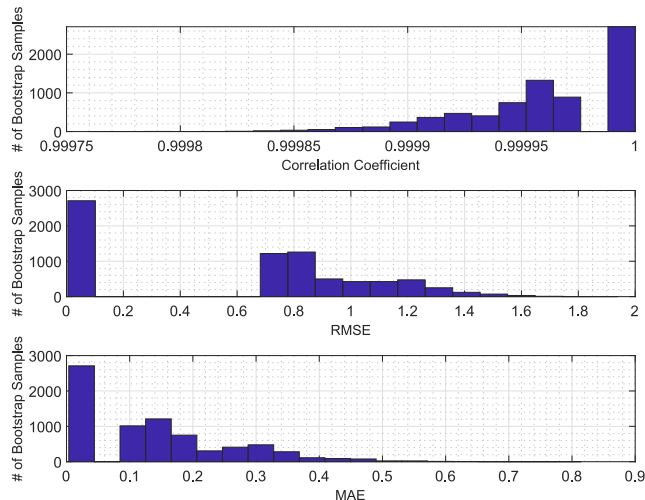


Fig. 4. Bootstrap analysis of GPR prediction stability. 7500 bootstrap samples are drawn with replacements from the whole sample. Each bootstrap sample is used to train the GPR based on the Rational Quadratic kernel and Constant basis function with lattice parameters standardized, and obtain the associate model performance. The histograms show distributions of the CC, RMSE, and MAE over the 7500 bootstrap samples, whose averages are 99.99%, 0.6190, and 0.1398, respectively.

Appendix A. Supplementary data

Supplementary data associated with this article can be found, in the online version, at <https://doi.org/10.1016/j.jmmm.2020.166998>.

Table 2
GPR prediction sensitivities to kernel choices.

Kernel	Basis Function	CC	RMSE	$\frac{RMSE}{Sample\ Mean}$	MAE	$\frac{MAE}{Sample\ Mean}$
Rational	Constant	99.99%	1.3453	0.59%	0.7869	0.35%
Quadratic						
Exponential	Constant	99.99%	1.3576	0.60%	0.7903	0.35%

Notes: The final GPR model is based on the Rational Quadratic kernel and Constant basis function. Detailed predictions from the GPR model based on the Exponential kernel and Constant basis function are also visualized in Fig. 3.

References

- [1] O. Gutfleisch, M.A. Willard, E. Brück, C.H. Chen, S.G. Sankar, J.P. Liu, Magnetic materials and devices for the 21st century: stronger, lighter, and more energy efficient, *Adv. Mater.* 23 (7) (2011) 821–842.
 - [2] M.H. Phan, S.C. Yu, Review of the magnetocaloric effect in manganite materials, *J. Magn. Magn. Mater.* 308 (2) (2007) 325–340.
 - [3] K.G. Sandeman, Magnetocaloric materials: the search for new systems, *Scr. Mater.* 67 (6) (2012) 566–571.
 - [4] R. Gimaev, Y. Spichkin, B. Kovalev, K. Kamilov, V. Zverev, A. Tishin, Review on magnetic refrigeration devices based on HTSC materials, *Int. J. Refrig.* (2019).
 - [5] J. Schwartz, T. Effo, X. Liu, Q.V. Le, A.L. Mbaruku, H.J. Schneider-Muntau, T. Shen, H. Song, U.P. Trociewitz, X. Wang, H.W. Weijers, High field superconducting solenoids via high temperature superconductors, *IEEE Trans. Appl. Supercond.* 18 (2) (2008) 70–81.
 - [6] J. Schwartz, C.C. Koch, Y. Zhang, X. Liu, Formation of bismuth strontium calcium copper oxide superconductors, U.S. Patent US9773962B2, September 26, 2017. <https://patents.google.com/patent/US9773962B2/en>.
 - [7] Y. Zhang, S. Johnson, G. Naderi, M. Chaubal, A. Hunt, J. Schwartz, High critical current density $\text{Bi}_2\text{Sr}_x\text{CaCu}_2\text{O}_x/\text{Ag}$ wire containing oxide precursor synthesized from nano-oxides, *Supercond. Sci. Technol.* 29 (9) (2016) 095012.
 - [8] Y. Zhang, C.C. Koch, J. Schwartz, "Formation of $\text{Bi}_2\text{Sr}_x\text{CaCu}_2\text{O}_x/\text{Ag}$ multi-filamentary metallic precursor powder-in-tube wires, *Supercond. Sci. Technol.* 29 (12) (2016) 125005.
 - [9] Y. Zhang, C.C. Koch, J. Schwartz, Synthesis of $\text{Bi}_2\text{Sr}_2\text{CaCu}_2\text{O}_x$ superconductors via direct oxidation of metallic precursors, *Supercond. Sci. Technol.* 27 (5) (2014)

- 055016.
- [10] V. Franco, J.S. Blázquez, J.J. Ipus, J.Y. Law, L.M. Moreno-Ramírez, A. Conde, Magnetocaloric effect: from materials research to refrigeration devices, *Prog. Mater. Sci.* 93 (2018) 112–232.
- [11] L. Lin, C. Gu, J. Zhu, Q. Ye, E. Jiang, W. Wang, M. Liao, Z. Yang, Y. Zeng, J. Sheng, W. Guo, Engineering of hole-selective contact for high-performance perovskite solar cell featuring silver back-electrode, *J. Mater. Sci.* 54 (10) (2019) 7789–7797.
- [12] J. Töpfer, J.B. Goodenough, LaMn_{3+δ}Revisited, *J. Solid State Chem.* 130 (1) (1997) 117–128.
- [13] R. Thiagarajan, S. Esakki Muthu, R. Mahendiran, S. Arumugam, Effect of hydrostatic pressure on magnetic and magnetocaloric properties of Mn-site doped perovskite manganites Pr_{0.6}Ca_{0.4}Mn_{0.96}B_{0.04}O₃ (B=Co and Cr), *J. Appl. Phys.* 115 (4) (2014) 043905.
- [14] M. Li, Z. Wang, Y. Wang, J. Li, D. Viehland, Giant magnetoelectric effect in self-biased laminates under zero magnetic field, *Appl. Phys. Lett.* 102 (8) (2013) 082404.
- [15] T. Mukherjee, S. Sahoo, R. Skomski, D.J. Sellmyer, C. Binek, Magnetocaloric properties of Co/Cr superlattices, *Phys. Rev. B* 79 (14) (2009) 144406.
- [16] V.S. Kumar, R. Chukka, Z. Chen, P. Yang, L. Chen, Strain dependent magnetocaloric effect in La_{0.67}Sr_{0.33}MnO₃ thin-films, *AIP Adv.* 3 (5) (2013) 052127.
- [17] Y. Wang, M. Li, D. Hasanyan, J. Gao, J. Li, D. Viehland, Geometry-induced magnetoelectric effect enhancement and noise floor reduction in Metglas/piezofiber sensors, *Appl. Phys. Lett.* 101 (9) (2012) 092905.
- [18] Q. Zhang, S. Thota, F. Guillou, P. Padhan, V. Hardy, A. Wahl, W. Prellier, Magnetocaloric effect and improved relative cooling power in (La_{0.7}Sr_{0.3}MnO₃/SrRuO₃) superlattices, *J. Phys.: Condens. Matter* 23 (5) (2011) 052201.
- [19] K. Abdouli, W. Cherif, H. Omrani, M. Mansouri, M.A. Valent, M.P.F. Graça, L. Ktari, Structural, magnetic and magnetocaloric properties of La_{0.5}Sm_{0.2}Sr_{0.3}Mn_{1-x}Fe_xO₃ compounds with (0≤x≤0.15), *J. Magn. Magn. Mater.* 475 (2019) 635–642.
- [20] H. Ben Khelifa, Y. Regaieg, W. Cheikhrouhou-Koubaa, M. Koubaa, A. Cheikhrouhou, Structural, magnetic and magnetocaloric properties of K-doped Pr_{0.8}Na_{0.2-x}K_xMnO₃ manganites, *J. Alloy. Compd.* 650 (2015) 676–683.
- [21] A. Bettaihi, R. M'hassri, A. Selmi, H. Rahmouni, N. Chniba-Boudjada, A. Cheikhrouhou, K. Khrisouni, Effect of chromium concentration on the structural, magnetic and electrical properties of praseodymium-calcium manganite, *J. Alloys Compd.* 650 (2015) 268–276.
- [22] S. Hcini, M. Boudard, S. Zemni, M. Oumezzine, Effect of Fe-doping on structural, magnetic and magnetocaloric properties of Nd_{0.67}Ba_{0.33}Mn_{1-x}Fe_xO₃ manganites, *Ceram. Int.* 40 (10) (2014) 16041–16050.
- [23] A. Jerbi, A. Krichene, N. Chniba-Boudjada, W. Boujelben, Magnetic and magnetocaloric study of manganite compounds Pr_{0.5}A_{0.05}Sr_{0.45}MnO₃ (A = Na and K) and composite, *Physica B* 477 (2015) 75–82.
- [24] M. Khelifi, M. Bejar, O.E. Sadek, E. Dahri, M.A. Ahmed, E.K. Hlil, Structural, magnetic and magnetocaloric properties of the lanthanum deficient in La_{0.8}Ca_{0.2-x}MnO₃ (x = 0–0.20) manganite oxides, *J. Alloys Compd.* 509 (27) (2011) 7410–7415.
- [25] S. Mahjoub, M. Baazaoui, R. M'nassri, H. Rahmouni, N.C. Boudjada, M. Oumezzine, Effect of iron substitution on the structural, magnetic and magnetocaloric properties of Pr_{0.6}Ca_{0.1}Sr_{0.3}Mn_{1-x}Fe_xO₃ (0≤x≤0.075) manganites, *J. Alloys Compd.* 608 (2014) 191–196.
- [26] A. Meleki, S. Othmani, W. Cheikhrouhou-Koubaa, M. Koubaa, A. Cheikhrouhou, E.K. Hlil, Effect of praseodymium doping on the structural, magnetic and magnetocaloric properties of Sm_{0.55-x}Pr_xSr_{0.45}MnO₃ (0.1≤x≤0.4) manganites, *J. Alloys Compd.* 645 (2015) 559–565.
- [27] P. Nisha, S.S. Pillai, M.R. Varma, K.G. Suresh, Critical behavior and magnetocaloric effect in La_{0.67}Ca_{0.33}Mn_{1-x}Cr_xO₃ (x = 0.1, 0.25), *Solid State Sci.* 14 (1) (2012) 40–47.
- [28] E. Oumezzine, S. Hcini, E.K. Hlil, E. Dahri, M. Oumezzine, Effect of Ni-doping on structural, magnetic and magnetocaloric properties of La_{0.6}Pr_{0.1}Ba_{0.3}Mn_{1-x}Ni_xO₃ nanocrystalline manganites synthesized by Pechini sol-gel method, *J. Alloys Compd.* 615 (2014) 553–560.
- [29] A. Selmi, R. M'nassri, W. Cheikhrouhou-Koubaa, N.C. Boudjada, A. Cheikhrouhou, Influence of transition metal doping (Fe, Co, Ni and Cr) on magnetic and magnetocaloric properties of Pr_{0.7}Ca_{0.3}MnO₃ manganites, *Ceram. Int.* 41(8) (2015) 10177–10184.
- [30] A. Selmi, R. M'nassri, W. Cheikhrouhou-Koubaa, N.C. Boudjada, A. Cheikhrouhou, Effects of partial Mn-substitution on magnetic and magnetocaloric properties in Pr_{0.7}Ca_{0.3}Mn_{0.95}O₅ (Cr, Ni, Co and Fe) manganites, *J. Alloys Compd.* 619 (2015) 627–633.
- [31] A. Selmi, R. M'nassri, W. Cheikhrouhou-Koubaa, N.C. Boudjada, A. Cheikhrouhou, The effect of Co doping on the magnetic and magnetocaloric properties of Pr_{0.7}Ca_{0.3}Mn_{1-x}Co_xO₃ manganites, *Ceram. Int.* 41(6) (2015) 7723–7728.
- [32] V. Basso, G. Bertotti, M. LoBue, C.P. Sasso, Theoretical approach to the magnetocaloric effect with hysteresis, *J. Magn. Magn. Mater.* 290 (2005) 654–657.
- [33] V. Franco, J.S. Blázquez, A. Conde, Field dependence of the magnetocaloric effect in materials with a second order phase transition: a master curve for the magnetic entropy change, *Appl. Phys. Lett.* 89 (22) (2006) 222512.
- [34] V. Franco, T. Gottschall, K.P. Skokov, O. Gutfleisch, First-order reversal curve (FORC) analysis of magnetocaloric heusler-type alloys, *IEEE Magn. Lett.* 7 (2016) 1–4.
- [35] M. Mihalik, J. Vejpravová, J. Rusz, M. Diviš, P. Svoboda, V. Sechovsky, M. Mihalik, Anisotropic magnetic properties and specific-heat study of a TbFe₂Si₂ single crystal, *Phys. Rev. B* 70 (13) (2004) 134405.
- [36] Y. Zhang, X. Xu, Yttrium barium copper oxide superconducting transition temperature modeling through Gaussian process regression, *Comput. Mater. Sci.* 179 (2020) 109583.
- [37] Y. Zhang, X. Xu, Predicting doped MgB₂ superconductor critical temperature from lattice parameters using Gaussian process regression, *Physica C* 573 (2020) 1353633.
- [38] Y. Zhang, X. Xu, Relative cooling power modeling of lanthanum manganites using Gaussian process regression, *RSC Adv.* (2020), <https://doi.org/10.1039/dra03031g> in press.
- [39] Y. Zhang, X. Xu, Gaussian process modeling of magnetocaloric lanthanum manganites Curie temperature, submitted for publication.
- [40] Y. Zhang, X. Xu, Machine learning the magnetocaloric effect in manganites from lattice parameters, *Appl. Phys. A* 126 (2020) 341.
- [41] Y. Zhang, X. Xu, Machine learning the magnetocaloric effect in manganites from compositions and structural parameters, *AIP Adv.* 10 (2020) 035220.
- [42] Y. Zhang, X. Xu, Predicting the thermal conductivity enhancement of nanofluids using computational intelligence, *Phys. Lett. A* 384 (2020) 126500.
- [43] Y. Zhang, X. Xu, Transformation temperature predictions through computational intelligence for NiTi-based shape memory alloys, submitted for publication.
- [44] Y. Zhang, X. Xu, Machine learning modeling of lattice constants for half-Heusler alloys, *AIP Adv.* 10 (2020) 045121.
- [45] Y. Zhang, X. Xu, Machine learning modeling of metal surface energy, submitted for publication.
- [46] Y. Zhang, X. Xu, Machine learning optical band gaps of doped-ZnO films, *Optik* 217C (2020) 164808, , <https://doi.org/10.1016/j.ijleo.2020.164808>.
- [47] Y. Zhang, X. Xu, Machine learning band gaps of doped-TiO₂ photocatalysts from structural and morphological parameters, submitted for publication.
- [48] A.E.R.T. AboZied, A.A. Ghani, A.I. Ali, T.A. Salaheldin, Structure, magnetic and magnetocaloric properties of nano crystalline perovskite La_{0.8}Ag_{0.2}MnO₃, *J. Magn. Magn. Mater.* 479 (2019) 266–267.
- [49] A.O. Ayaş, S.K. Çetin, M. Akyol, G. Akça, A. Ekicibil, Effect of B site partial Ru substitution on structural magnetic and magnetocaloric properties in La_{0.7}Pb_{0.2}Mn_{1-x}Ru_xO₃ (x = 0, 0.1 and 0.2) perovskite system, *J. Mol. Struct.* 1200 (2020) 127120.
- [50] S. Banik, K. Das, I. Das, Enhancement of magnetoresistance and magnetocaloric effect at room temperature in polycrystalline Pr_{0.8-x}La_xSr_{0.2}MnO₃ (x = 0.2) compound, *J. Magn. Magn. Mater.* 490 (2019) 165443.
- [51] R. Bellouz, M. Oumezzine, E.K. Hlil, E. Dahri, Critical behavior near the ferromagnetic-paramagnetic phase transition in La_{0.65}Eu_{0.05}Sr_{0.3}Mn_{1-x}Cr_xO₃ (x = 0.10 and x = 0.15), *Physica B* 456 (2015) 93–99.
- [52] E. Bouzaïene, A.H. Dahri, J. Dahri, E.K. Hlil, A. Bahajzar, Effect of A-site-substitution on structural, magnetic and magnetocaloric properties in La_{0.7}Ca_{0.3}Mn_{0.9}Cu_{0.1}O₃ manganite, *J. Magn. Magn. Mater.* 491 (2019) 165540.
- [53] S.K. Çetin, G. Akça, A. Ekicibil, Impact of small Er rare earth element substitution on magnetocaloric properties of (La_{0.9}Er_{0.1})_{0.67}Pb_{0.33}MnO₃ perovskite, *J. Mol. Struct.* 1196 (2019) 658–661.
- [54] R. Cherif, E.K. Hlil, M. Ellouze, F. Elhalouani, S. Obbade, Magnetic and magnetocaloric properties of La_{0.6}Pr_{0.1}Sr_{0.3}Mn_{1-x}Fe_xO₃ (0≤x≤0.3) manganites, *J. Solid State Chem.* 215 (2014) 271–276.
- [55] K. Das, N. Banu, I. Das, B.N. Dev, Significantly large magnetocaloric effect in polycrystalline La_{0.8}Sr_{0.17}MnO₃ near room temperature, *Physica B* 545 (2018) 438–441.
- [56] A. Dahri, F.I.H. Rhouma, S. Mnefgui, J. Dahri, E.K. Hlil, Room temperature critical behavior and magnetocaloric properties of La_{0.6}Nd_{0.1}(CaSr)_{0.3}Mn_{0.9}V_{0.1}O₃, *Ceram. Int.* 40 (1) (2014) 459–464.
- [57] S. Ghodbane, E. Tka, J. Dahri, E.K. Hlil, A large magnetic entropy change near room temperature in La_{0.8}Ba_{0.1}Ca_{0.1}Mn_{0.97}Fe_{0.03}O₃ perovskite, *J. Alloy. Compd.* 600 (2014) 172–177.
- [58] S. Kallel, N. Kallel, O. Peña, M. Oumezzine, Large magnetocaloric effect in Ti-modified La_{0.70}Sr_{0.30}MnO₃ perovskite, *Mater. Lett.* 64 (9) (2010) 1045–1048.
- [59] S. Kallel, N. Kallel, A. Hagaza, O. Peña, M. Oumezzine, Large magnetic entropy change above 300 K in (La_{0.56}Ce_{0.14})Sr_{0.3}MnO₃ perovskite, *J. Alloys Compd.* 492 (1–2) (2010) 241–244.
- [60] S.E. Kossi, S. Ghodbane, S. Mnefgui, J. Dahri, E.K. Hlil, The impact of disorder on magnetocaloric properties in Ti-doped manganites of La_{0.7}Sr_{0.25}Na_{0.05}Mn_(1-x)Ti_xO₃ (0≤x≤0.2), *J. Magn. Magn. Mater.* 395 (2015) 134–142.
- [61] K. Laajimi, M. Khelifi, E.K. Hlil, M.H. Gazzah, J. Dahri, Enhancement of magnetocaloric effect by Nickel substitution in La_{0.65}Ca_{0.33}Mn_{0.98}Ni_{0.02}O₃ manganite oxide, *J. Magn. Magn. Mater.* 491 (2019) 165625.
- [62] V.Y. Mitrofanov, S.K. Estemirova, G.A. Kozhina, Effect of oxygen content on structural, magnetic and magnetocaloric properties of (La_{0.7}Pr_{0.3})_{0.8}Sr_{0.2}Mn_{0.9}Co_{0.1}O_{3±δ}, *J. Magn. Magn. Mater.* 476 (2019) 199–206.
- [63] M. Mohamed, M. Mohamed, M. Khitouni, N. Ramneh, Effects of partial Li-substitution on magnetic and magnetocaloric properties in New perovskite La_{1-x}Li_xSrMn₂O_{5+δ}, *J. Mol. Struct.* 1202 (2020) 127187.
- [64] M. Oumezzine, S. Zemni, O. Peña, M. Oumezzine, S. Zemni, and O. Peña, “Room temperature magnetic and magnetocaloric properties of La_{0.67}Ba_{0.33}Mn_{0.98}Ti_{0.02}O₃ perovskite, *J. Alloys Compd.* 508 (2) (2010) 292–296.
- [65] T.L. Phan, P.Q. Thanh, N.H. Sinh, K.W. Lee, S.C. Yu, Critical behavior and magnetic entropy change in La_{0.7}Ca_{0.3}Mn_{0.9}Zn_{0.1}O₃ perovskite manganite, *Curr. Appl. Phys.* 11 (3) (2011) 830–833.
- [66] A. Rostamnejadi, M. Venkatesan, P. Kameli, H. Salamat, J.M.D. Coey, Magnetocaloric effect in La_{0.65}Sr_{0.33}MnO₃ manganite above room temperature, *J. Magn. Magn. Mater.* 323 (16) (2011) 2214–2218.
- [67] R. Skini, A. Omri, M. Khelifi, E. Dahri, E.K. Hlil, Large magnetocaloric effect in lanthanum-deficiency manganites La_{0.8-x}Ca_{0.2}MnO₃ (0.00≤x≤0.20) with a first-order magnetic phase transition, *J. Magn. Magn. Mater.* 364 (2014) 5–10.
- [68] R. Skini, M. Khelifi, E. Dahri, E.K. Hlil, Lanthanum deficiency effect on the structural, magnetic, and transport properties of the La_{0.8-x}Ca_{0.2}MnO₃ manganites

- oxides, *J. Supercond. Novel Magn.* 27(1), 247–256.
- [69] C.A. Taboada-Moreno, F. Sánchez-De Jesús, F. Pedro-García, C.A. Cortés-Escobedo, J.A. Betancourt-Cantera, M. Ramírez-Cardona, A.M. Bolarín-Miró, Large magnetocaloric effect near to room temperature in Sr doped $\text{La}_{0.7}\text{Ca}_{0.3}\text{MnO}_3$, *J. Magn. Magn. Mater.* 496 (2020) 165887.
- [70] E. Tka, K. Cherif, J. Dhahri, Evolution of structural, magnetic and magnetocaloric properties in Sn-doped manganites $\text{La}_{0.57}\text{Nd}_{0.1}\text{Sr}_{0.33}\text{Mn}_{1-x}\text{Sn}_x\text{O}_3$ ($x = 0.05\text{--}0.3$), *Appl. Phys. A* 116(3) (2014) 1181–1191.
- [71] Z. Wang, J. Jiang, Magnetic entropy change in perovskite manganites $\text{La}_{0.7}\text{A}_{0.3}\text{MnO}_3\text{La}_{0.7}\text{A}_{0.3}\text{Mn}_{0.9}\text{Cr}_{0.1}\text{O}_3$ ($\text{A} = \text{Sr}, \text{Ba}, \text{Pb}$) and Banerjee criteria on phase transition, *Solid State Sci.* 18 (2013) 36–41.
- [72] N. Zaidi, S. Mnefgui, A. Dhahri, E.K. Hlil, J. Dhahri, Critical parameters near the phase transition temperature in $\text{La}_{0.67-x}\text{Dy}_x\text{Pb}_{0.33}\text{MnO}_3$, *J. Rare Earths* 33 (2) (2015) 168–176.